Israel Journal of Chemistry *Vol. 49* *2009* *pp. 187–197*
DOI: 10.1560/IJC.49.2.187

Quantum Dynamics of the Excited-State Intramolecular Proton Transfer in 2-(2′-Hydroxyphenyl)benzothiazole

Justin Kim,[a] Yinghua Wu,[b] Jean-Luc Brédas,[b] and Victor S. Batista[a,*]
[a]Department of Chemistry, Yale University, P.O. Box 208107, New Haven, Connecticut 06520-8107, USA
[b]Department of Chemistry, Georgia Institute of Technology, 901 Atlantic Drive NW, Atlanta, Georgia 30332-0400, USA

(Received 31 December 2008 and in revised form 30 April 2009)

Abstract. The excited-state intramolecular proton-transfer dynamics and photoabsorption associated with the ketoenolic tautomerization reaction in 2-(2′-hydr oxyphenyl)benzothiazole are simulated according to a numerically exact quantum-dynamics propagation method and a full-dimensional excited-state potential energy surface based on an ab initio reaction surface Hamiltonian. The simulations involve the propagation of 69-dimensional wave packets according to the matching-pursuit/split-operator Fourier transform (MP/SOFT) method (Wu, Y.; Batista, V.S. *J. Chem. Phys.* **2004**, *121*, 1676–1686). The underlying propagation scheme recursively applies the time-evolution operator as defined by the Trotter expansion to second-order accuracy in dynamically adaptive coherent-state expansions. Computations of time-dependent survival amplitudes, the time-dependent product population, and photoabsorption linewidths are compared to experimental data. The reported results provide fundamental insight on the nature of the excited-state reaction dynamics and demonstrate the capabilities of the MP/SOFT method as a powerful computational tool to study ultrafast reaction dynamics in polyatomic systems.

INTRODUCTION

Excited-state intramolecular proton transfer (ESIPT) reactions are important for a wide range of systems in biological processes[1–3] and technological developments,[4] such as photostabilizers[5] and UV filter materials.[6] These are usually ultrafast reactions in excited electronic states that require detailed investigations based on state-of-the-art spectroscopic and computational methods. This paper reports for the first time full-dimensional quantum dynamics simulations of the ESIPT associated with the enol–keto tautomerization reaction in 2-(2′-hydroxyphenyl)benzothiazole (HBT) (see Fig. 1). The simulations are based on the recently developed matching-pursuit/split-operator-Fourier transform (MP/SOFT) method,[7–11] applied in conjunction with an ab initio reaction surface Hamiltonian.[12–16]

In recent years, there has been significant interest in studies of organic molecules exhibiting photoinduced ESIPT in keto-enolic tautomerization reactions, including experimental[17–33] and theoretical[14,16,34–43] work. In particular, the ultrafast ESIPT reaction of HBT has been investigated by several experimental studies based on pump–probe techniques.[17–24] The reaction is described by the four-step photophysical scheme depicted in Fig. 1. The enol-to-keto transformation takes place in the excited electronic state, after ultraviolet photoexcitation of the ground-state enol form. The keto form relaxes to the ground state by fluorescence emission, and the enol form is recovered spontaneously by reverse proton transfer, completing the cycle. Along the proton

*Author to whom correspondence should be addressed.
E-mail: victor.batista@yale.edu

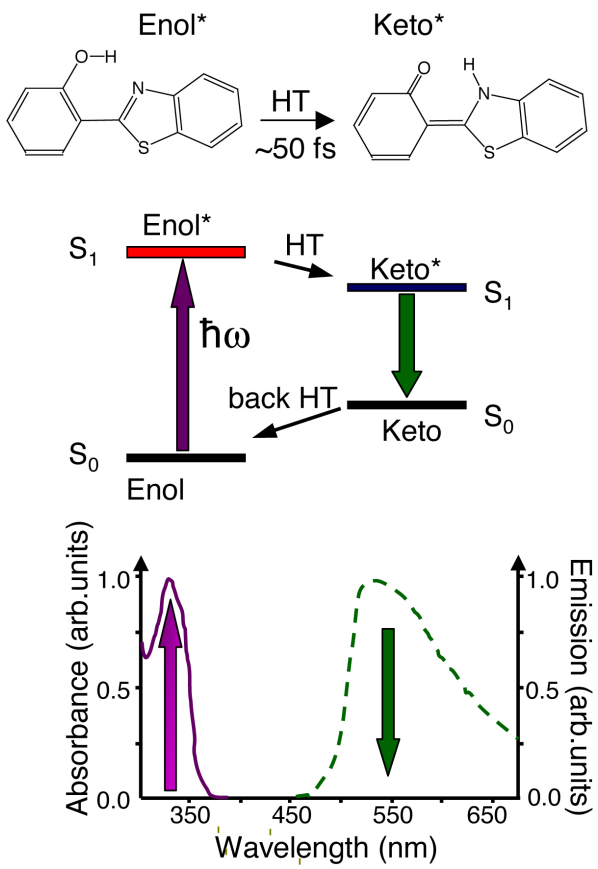

Fig. 1. Molecular structural diagram describing the ultrafast hydrogen transfer (HT) due to enol–keto tautomerization in 2-(2′-hydroxyphenyl)benzothiazole (HBT), after ultraviolet π–π* electronic excitation of the enol state (purple arrow). The keto*–S_1 state decays (green arrow) on subnanosecond time scales to the enol–S_0 state by fluorescence photoemission. The optical spectra show a large Stokes-shift between the photoabsorption (purple) and fluorescence (green) bands, typical of excited-state hydrogen/proton transfer reactions.[17,22,23]

transfer process, distinctive transient IR absorptions and fluorescence emission with large Stokes shifts can be observed as direct evidence of proton transfer and formation of the keto form, including C=O-stretching vibrations characteristic of the keto tautomer.[17–24] Like many other intramolecular proton transfer systems,[24,44,45] both the absorption and emission spectra show negligible shifts due to solvent effects,[17–24] indicating that the ultrafast excited-state dynamics is rather insensitive to the surrounding molecular environment. Therefore, gas-phase simulations should provide realistic descriptions of the underlying quantum reaction dynamics.

The first ultrafast spectroscopic study of enol–keto tautomerization in HBT focused on the analysis of changes in the OH-stretching band, centered at 3000 cm^{-1}, and in the fingerprint region between 1400 and 2000 cm^{-1} in an effort to characterize changes in the molecular configuration induced by hydrogen transfer.[17] Subsequently, femtosecond IR spectroscopy monitored the fingerprint bands, after photoexcitation with the UV pump tuned between 310 and 350 nm.[22,23] The IR absorption at 1530 cm was assigned to the carbonyl-stretching mode, significantly red-shifted due to intramolecular hydrogen-bonding and coupling to the larger conjugated π-electronic system. These experimental studies concluded that the formation of the keto state was characterized by the rise of the carbonyl-stretching band, within about 50 fs after UV excitation of the enol tautomer. These results suggested that the ESIPT reaction could not be explained in terms of a simple OH-stretching motion since the (50 fs) time scale is much slower than the (4 fs) half-period of the OH-stretching.[22,23] A tentative explanation based on the coherent effects of anharmonic coupling to low frequency (60 and 120 cm^{-1}) modes suggested that the ESIPT could be coupled to out-of-plane deformation by nonradiative processes within the excited enol state.[22,23] However, the detailed nature of the underlying relaxation process could not be extracted from cursory examination of the experimental data.[22,23] In this paper, we simulate the enol-to-keto transfer dynamics on the excited state potential energy surface (PES) according to a rigorous time-dependent wave packet propagation method, and we show that the reported reaction time scales are consistent with experimental data. The proton motion is analyzed as correlated with the rearrangement of electronic charge density in an effort to characterize the net transfer of a hydrogen atom (i.e., ESIHT),[18,19] as resulting from ESIPT coupled to photoinduced electron transfer.

Theoretical studies of ESIPT reactions in polyatomic molecules are particularly challenging since the proton quantum motion is often coupled to the reorganization of lower-frequency vibrational modes.[13–16] A rigorous first-principle description of reaction dynamics requires first computing the ab initio PESs and then solving accurately the equations of motion on these surfaces by explicitly integrating the time-dependent Schrödinger equation. In recent years, there has been significant progress in the development and application of computational methods for quantum dynamical processes,[7–11,46–70] including numerically exact methods[71–83] based on the split operator Fourier transform method,[84–86] the Chebyshev expansion,[87] or short iterative Lanczos methods,[88] and semiclassical methods such as the Herman–Kluk method[89] and the forward–backward semiclassical method.[90] However, rigorous quantum dynamical simulations for

the size of molecules involved in ESIPT processes are usually hindered by the demands of computational effort of quantum propagation methods. Recently, the MP/SOFT method has been introduced as a practical and rigorous time-dependent scheme for simulations of quantum processes in multidimensional systems.[7–11] It has been applied to a number of model Hamiltonians, as well as to the simulation of the ESIPT reaction in 2-(2′-hydroxyphenyl)oxazole (HPO), explicitly treating 35 coupled degrees of freedom.[15] In this paper, we apply the MP/SOFT methodology to report the full 69-dimensional quantum dynamical simulation of the ESIPT in HBT, including the description of hydrogen transfer explicitly coupled to the redistribution of electronic charge and the motion of the remaining degrees of freedom in the system.

The MP/SOFT method[7–11] is based on the recursive application of the time evolution operator, as defined by the Trotter expansion to the second-order accuracy, in non-orthogonal and dynamically adaptive coherent-state representations generated according to the matching-pursuit algorithm.[91] The coherent state representations allow for the analytic implementation of the Trotter expansion, by-passing the exponential scaling problem associated with the fast Fourier transform algorithm in standard grid-based SOFT approaches. One of the advantages of MP/SOFT relative to other time-dependent methods[47,50,92–101] is that the method is easier to implement since it avoids the usual need of solving a coupled system of differential equations for propagating expansion coefficients. The method is most efficient when applied in conjunction with reaction surface Hamiltonians[12] since the multidimensional integrals necessary to generate the coherent-state expansions can be efficiently computed.[14–16] In this paper, we have adopted this type of coupled system-bath Hamiltonians to model the PES where the OH-stretching mode and the internal bending mode of 120 cm are identified as the quantum reaction coordinates, while the other vibrational modes are described as harmonic oscillators with equilibrium coordinates parametrized by the reaction coordinates. The MP/SOFT simulations are compared to experiments and the description of reaction dynamics provided by the mixed quantum-classical time-dependent self-consistent field method (TDSCF),[102] in which the reaction coordinates are treated quantum mechanically and the other modes classically.

The paper is organized as follows. First, we briefly introduce the MP/SOFT method, and the calculations of the absorption spectrum and the time-dependent product population. Then, we present the simulation results and the comparisons to the experimental data. Finally, we summarize and conclude.

METHODS

Excited-State Potential Energy Surface

The ab initio S_1 PES of HBT has been constructed by using the reaction surface approach,[12] as implemented in earlier studies of ESIPT.[13–16] The reaction coordinates r_1 and r_2 were identified as the normal modes with predominant components along the OH-stretching mode and the CCC internal bending mode (120 cm) that modulates the distance between the proton donor and acceptor moieties. The other 67 vibrational modes were described as locally harmonic oscillators with ab initio force constants $\mathbf{F}(r_1,r_2)$ and equilibrium positions $\mathbf{z}_0(r_1,r_2)$ parameterized by the reaction coordinates r_1 and r_2. The resulting 69-dimensional potential energy surface is

$$V(r_1,r_2,\mathbf{z}) = V_0(r_1,r_2) + \frac{1}{2}[\mathbf{z}-\mathbf{z}_0(r_1,r_2)]\mathbf{F}(r_1,r_2)[\mathbf{z}-\mathbf{z}_0(r_1,r_2)] \quad (1)$$

where $V_0(r_1,r_2)$ is the reaction surface obtained by fully optimizing the geometry of the system with respect to all nuclear coordinates, subject to the constraints of fixed values of r_1 and r_2 (see Fig. 2). The equilibrium coordinates $\mathbf{z}_0(r_1,r_2)$ of the bath modes are the normal mode

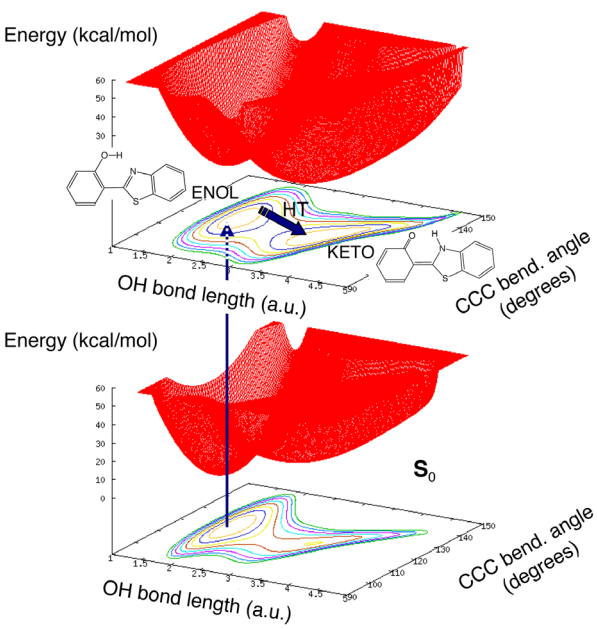

Fig. 2. Potential energy surfaces $V_0(r_1, r_2)$ of the S_0 and S_1 electronic states of HBT, as a function of the reaction coordinates introduced in the text. The contour lines are equally spaced at 5 kcal mol^{-1}. The vertical arrow indicates the instantaneous $S_1 \leftarrow S_0$ ultraviolet photoexcitation. The thick blue arrow indicates the hydrogen transfer (HT) after photoexcitation of the enol tautomer.

displacements relative to the reference ground-state minimum energy configuration. All excited-state minimum energy structures were obtained at the CIS/6-31G* level of theory, as implemented in Gaussian 03.[103]

The comparative analysis of the $V_0(r_1,r_2)$ PESs for the S_0 and S_1 states (see Fig. 2) shows that the HT energy barriers in the S_1 state are significantly lower than in the S_0. In addition, the minimum energy configuration of HBT in the enol-S_1 state is shifted relative to the initial equilibrium position in the S_0 state. Therefore, the vertical transition due to ultraviolet photoexcitation leaves the wave packet in the S_1 in a configuration that is displaced relative to the S_1 equilibrium geometry. The ensuing coherent vibrations exchange energy with the OH coordinate, modulating hydrogen transfer each time the proton donor hydroxyphenyl and exceptor benzothiazole moieties are brought closer together.

MP/SOFT Method

A thorough description of the MP/SOFT method can be found in previous work.[7–11] Here, we present only a brief outline of the method with emphasis on how to implement it to simulate the ESIPT in HBT.

The initial nuclear wave packet $|\Psi_0\rangle = \varepsilon_0 \cdot \hat{\mu}\,|\Phi_0\rangle$ in the S_1 electronic state is modeled as obtained by ultraviolet photoexcitation of HBT initially prepared in the ground vibrational state of the S_0 electronic state, with $\hat{H}\,|\Phi_0\rangle = E_0\,|\Phi_0$. Under the Franck–Condon principle (i.e., with the electronic transition dipole moment $\langle S_1|\,\hat{\mu}\,|S_0\rangle$ assumed to be independent of the nuclear coordinates) $|\Psi_0\rangle$ can be modeled by the harmonic approximation:

$$\langle \mathrm{x} \mid \Psi_0 \rangle \prod_{j=1}^{69} \left(\frac{\alpha_j}{\pi}\right)^{1/4} \exp\left(-\frac{1}{2}\alpha_j \mathrm{x}_j^2\right) \tag{2}$$

where $\alpha_j = \omega_j m_j$, with m_j the reduced mass and ω_j the frequency of the normal mode j, obtained from the ab initio B3LYP/6-31G* normal mode analysis.

The time-evolved wave packet is calculated by recursively applying the short-time approximation to the time-evolution operator as defined by the Trotter expansion to the second-order accuracy:

$$e^{-i\hat{H}\tau} \approx e^{-iV(\hat{x})\tau/2} e^{-i\frac{\hat{p}^2}{2m}\tau} e^{-iV(\hat{x})\tau/2} \tag{3}$$

Here, τ is a short propagation time-period for the evolution of the system as described by the Hamiltonian $\hat{H} = \hat{\mathbf{p}}^2/(2m) + V(\hat{\mathrm{x}})$. To keep the notation as simple as possible, all expressions are written in mass-weighted coordinates $\mathrm{x} = (r_1, r_2, \mathbf{z})$ and atomic units, so that all degrees of freedom have the same mass m and $\hbar = 1$.

To implement the Trotter expansion, we first represent the state $|\tilde{\Psi}_t\rangle \equiv e^{-iV(x)\tau}|\Psi_t\rangle$ as a matching pursuit coherent-state expansion,[7–11]

$$|\tilde{\Psi}_t\rangle \sum_{j=1}^{n} c_j |j\rangle \tag{4}$$

where the expansion coefficients c_j are defined as follows: $c_1 \equiv \langle 1 \mid \tilde{\Psi}_t\rangle$ and $c_j \equiv \langle j \mid \tilde{\Psi}_t\rangle - \sum_{k=1}^{j-1} c_k \langle j \mid k\rangle$ for $j = 2$–n. The basis functions $\langle \mathrm{x} \mid j\rangle$ are 69-dimensional coherent states,

$$\langle \mathrm{x} \mid j \rangle \equiv \prod_{k=1}^{69} A_j(k) \mathrm{e}^{-\gamma_j(k)(x(k)-x_j(k))^2/2 + ip_j(k)(x(k)-x_j(k))} \tag{5}$$

with complex-valued coordinates $x_j(k) \equiv r_j(k) + id_j(k)$, momenta $p_j(k) \equiv g_j(k) + if_j(k)$, and scaling parameters $\gamma_j(k) \equiv a_j(k) + ib_j(k)$. The normalization constants are $A_j(k) \equiv (a_j(k)/\pi)^{1/4} \exp\Big[-\frac{1}{2}a_j(k)d_j(k)^2 - (d_j(k)g_j(k) - (b_j(k)d_j(k) + f_j(k))^2/(2a_j(k))\Big]$.

Once the coherent-state expansion of $|\tilde{\Psi}_{t0}\rangle$ is obtained, the time-evolved wave packet $|\Psi_{t+\tau}\rangle$ can be computed by applying the product of operators $e^{-iV(x)\tau} e^{-i\frac{\hat{p}^2}{2m}\tau}$, introduced by eq 3, as follows:

$$|\Psi_{t+\tau}\rangle \equiv e^{-iV(x)\tau} e^{-i\frac{\hat{p}^2}{2m}\tau} |\tilde{\Psi}_t = \sum_{j=1}^{n} c_j e^{-iV(x)\tau} |\tilde{j} \tag{6}$$

where

$$\langle \mathbf{x} \mid \tilde{j} \rangle \equiv \prod_{k=1}^{N} A_j(k) \sqrt{\frac{m}{m + i\tau\gamma_j(k)}} \exp\left[-\frac{\gamma_j(k)}{2} \frac{(x(k) - x_j(k))^2}{(1 + i\gamma_j(k)\tau/m)} + ip_j(k) \frac{(x(k) - x_j(k))}{(1 + i\gamma_j(k)\tau/m)} - i\frac{p_j^2(k)}{2m(1 + i\gamma_j(k)\tau/m)}\tau\right] \tag{7}$$

Further propagation of the resulting coherent-state expansion, introduced by eq 6, is analogously performed. Therefore, the underlying computational task necessary for quantum dynamics propagation is reduced to the recursive generation of matching pursuit coherent-state expansions as defined by eq 4.

Matching pursuit expansions are obtained by successive orthogonal projections of the target state onto coherent-state components. The first coherent state is selected by locally optimizing the position, width, and momentum parameters of a coherent state $|1\rangle$ that maximizes the overlap with the target wave function $\|\langle 1 \mid \tilde{\Psi}_t\rangle\|$ as follows:

$$|\tilde{\Psi}_t\rangle = c_1 |1\rangle + |e_1\rangle \tag{8}$$

where $c_1 \equiv \langle 1 \mid \tilde{\Psi}_t\rangle$. With this definition of c_1, the residue $|e_1\rangle$ is orthogonal to $|\tilde{\Psi}_t\rangle$. Therefore, $\| e_1 \| < \| \Psi \|$. Following the same procedure, we select the next coherent state $|2\rangle$ of the expansion as the one that best resembles the residue,

$$|e_1\rangle = c_2 |2\rangle + |e_2\rangle \tag{9}$$

where $c_2 \equiv \langle 2 \mid e_1\rangle$ *and* $\| e_1 \| > \| e_2 \|$. The sequential orthogonal projections are applied n times until the norm of the residue $\| e_n \|$ is smaller than the desired accuracy ϵ:

$$\| e_n \| = \sqrt{1 - \sum_{i=1}^{n} c_i^2} < \epsilon \tag{10}$$

The resulting expansion is

$$| \tilde{\Psi}_t \rangle = \sum_{j=1}^{n} c_j | j \rangle \tag{11}$$

with

$$c_1 \equiv \langle 1 | \tilde{\Psi}_t \rangle$$
$$c_j \equiv \langle j | \tilde{\Psi}_t \rangle - \sum_{k=1}^{j-1} c_k \langle j | k \rangle \, for \; j > 1 \tag{12}$$

The computational bottleneck of the MP/SOFT method involves the calculations of the overlap matrix elements $\langle j | e^{-i\hat{V}(x)\tau} | \tilde{k} \rangle$. For the S_1 PES of HBT, the partial integration with respect to the 67 harmonic modes **z** is performed analytically, while the integration with respect to the reaction coordinates r_1 and r_2 is efficiently performed according to numerical quadrature techniques.

RESULTS

The results are presented in three subsections. First, we present the photoabsorption spectrum calculated by MP/SOFT simulations of the enol–keto tautomerization reaction, as resulting from ultraviolet photoexcitation of the enol tautomer to the S_1 electronic excited state and the subsequent ultrafast ESIPT. Second, we present the results of MP/SOFT calculations of the time-dependent keto-S_1 population, as determined by ESIPT coupled to the motion of the remaining degrees of freedom in the system. Finally, we discuss the computational results as compared to experimental data.

Photoabsorption

The photoabsorption line width $I_0(\omega)$ at 0 K is computed as the Fourier transform of the survival amplitude $\xi(t) \equiv \langle \Psi_0 | e^{i\hat{H}t/\hbar} | \Psi_0 \rangle = \langle \Psi_0 | \Psi_t \rangle$,

$$I_0(\omega) = \frac{3}{2\pi\hbar} \int_{-\infty}^{\infty} dt e^{\frac{i}{\hbar}(\hbar\omega + E_0)t} \xi(t) e^{-|t|/T_2} \tag{13}$$

where $\omega = 2\pi c/\lambda$. E_0 is the initial energy of the system in the S_0 state and $T_2 = 40$ fs is a phenomenological dephasing constant that reproduces the inhomogeneous broadening of the spectrum of HBT in solutions.[18] The time-evolved wave function $|\Psi_t\rangle$ is obtained by MP/SOFT propagation of the initial state $|\Psi_0\rangle$, introduced by eq 2, according to the full-dimensional PES of the S_1 state introduced by eq 1.

Figure 3 shows that the calculated photoabsorption line width of HBT consists of a broad UV band with a very diffused superimposed vibronic structure that starts with the 0–0 transition at 3.34 eV. The maximum absorption is obtained at 344 nm (3.6 eV), which is lower than the vertical excitation at 3.89 eV and a little higher than the excitation from the ground-state enol form to the optimized enol form in the S_1 excited state at 3.57 eV. These results are in very good agreement with experimental data where the maximum absorption has been reported in the 330–350 nm range for HBT in nonpolar solvents.[17–19,22,23] Note that there has been no direct measurement of the 0–0 transition and a considerable energy difference exists between the 0–0 transition and the maximum absorption. Therefore, the agreement with experimental data suggests that the MP/SOFT methodology applied in conjunction with the full-dimensional system-bath model Hamiltonian can properly describe the ESIPT dynamics coupled to the motion of the remaining degrees of freedom in the system as well as the effect of the excited-state relaxation on the photoabsorption spectroscopy of HBT.

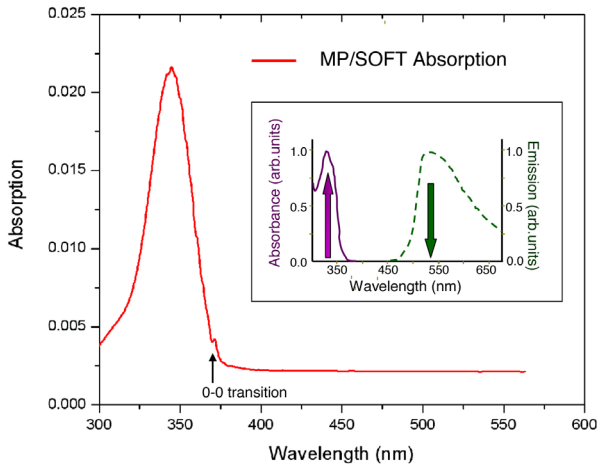

Fig. 3. Photoabsorption spectrum of HBT obtained according to the MP/SOFT method, as described in the text. For comparison, the inset shows the experimental photoabsorption and fluorescence bands as also shown in Fig. 1.[17,22,23]

Product Population and Decoherence

Figure 4 shows the time-dependent population $P_k(t) = Tr[h(r_1)\rho t(r_1)]$ of the keto product (red line) formed upon ultraviolet excitation of the enol tautomer. Here, $\rho t(r_1) = \int d\mathbf{z} \int dr_2 \Psi_t(r_1 r_2 \mathbf{z}) \Psi_t^*(r_1 r_2 \mathbf{z})$ is the reduced probability density associated with the proton position r_1, computed by squaring the 69-dimensional wave packet and integrating out the remaining degrees of freedom, including r_2 and **z**. The Heaviside step function $h(x)$ is defined as 1(0) on the product(reactant) side of the dividing transition-state surface separating the keto and enol configurations. Figure 4 also shows the comparison with the corresponding calculations based on the mixed quantum-classical TDSCF method (blue line).[102]

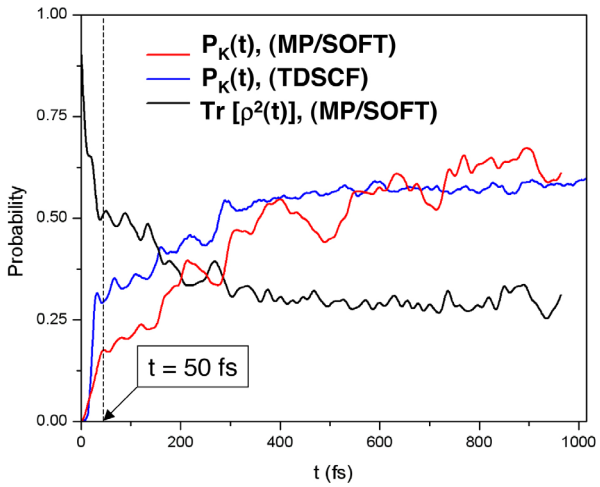

Fig. 4. Time-dependent product (keto tautomer) population $P_k(t) = Tr[h(r_1)\rho t(r_1)]$, where $h(x)$ is the Heaviside step function with value 1(0) on the product(reactant) side of the dividing transition-state surface, and $\rho t(r_1)$ is the MP/SOFT reduced probability density associated with the proton coordinate (red line). For comparison, analogous results were also obtained with the TDSCF approach (blue line). The time-dependent $Tr[\rho^2(t)]$ (black line) characterizes the extent and time scale of decoherence associated with proton motion.

The implementation of the TDSCF method is similar to our previous study of ESIPT in HPO,[15] and involves a single-configuration Hartree ansatz,

$$\Psi_t(R,\mathbf{z}) = e^{i\eta(t)}\chi_t(\mathbf{R})\phi_t(\mathbf{z}) \tag{14}$$

where $\eta(t)$ is an overall phase factor and $\mathbf{R} = (r_1,r_2)$ represents the reaction coordinates, including the OH-stretching mode r_1, and the 120 cm^{-1} in-plane hydroxyphenylbenzothiazole CCC-bending mode r_2. The remaining 67 vibrational modes are represented by the multidimensional coordinate $\mathbf{z}$.

Substituting the ansatz introduced by eq 14 into the time-dependent Schrödinger equation, we obtain the well-known self-consistent field equations,[102,104]

$$i\hbar\dot{\phi}_t(\mathbf{z}) = \langle \chi_t | \hat{H} | \chi_t \rangle \phi_t(\mathbf{z}) \tag{15}$$

and

$$i\hbar\dot{\chi}_t(\mathbf{R}) = \langle \phi_t | \hat{H} | \phi_t \rangle \chi_t(\mathbf{R}) \tag{16}$$

where $\phi_t(\mathbf{z})$ is approximated by the Gaussian wave packet,

$$\phi_t(\mathbf{z}) = \prod_{j=3}^{69} \pi^{-1/4} \exp\left(-\frac{1}{2}\left(z_j - \bar{z}_j(t)\right)^2 + \frac{i}{\hbar}\left(\bar{p}_j(t)\left(z_j - \bar{z}_j(t)\right) + S(t)\right)\right) \tag{17}$$

Here, $\{\bar{z}_j(t), \bar{p}_j(t)\}$ are classical coordinates and momenta evolving according to the effective potential energy surface $V_e(\mathbf{z};t) = \langle \chi_2 | \hat{H} | \chi_t \rangle$. These trajectories, as well as the classical action $S(t)$, are computed by numerically integrating Hamilton's equations according to the Velocity–Verlet algorithm.[105] Initial conditions are chosen by importance sampling Monte Carlo, with sampling functions defined by the initial Husimi distribution. Finally, χ_t is propagated according to the MP/SOFT methodology, integrating eq 3.4 self-consistently with eq 15. The initial conditions for the classical modes are sampled according to the Wigner distribution[106] based on the initial wave function defined in eq 2.

Both MP/SOFT and TDSCF calculations show similar time scales for the ultrafast formation of the keto tautomer in the S_1-state, as modulated by high-frequency modes, and the equilibration of the keto and enol populations within several hundreds of femtoseconds after photoexcitation of the system. Both calculations show evidence of multiple time scales, including the correlation of product formation with the coherent vibration of high frequency modes with a vibrational period of about 50 fs. Two distinctive reaction rates include the ultrafast transfer of 15–30% population in just 30–50 fs and further increase of the keto population, albeit with a much slower rate, to about 60% in the next 400–500 fs. After that the keto and enol populations equilibrate around this asymptotic level. The two time scales indicate that a small barrier exists along the OH reaction coordinate, separating the enol and keto tautomeric forms by a transition state on the S_1 PES. A small percentage of molecules with enough energy along the reaction coordinate transfers directly over the barrier, while most of the population with less energy than the barrier transfers only by tunneling in about 50 fs, or at later times after vibrational energy redistribution. Thus, the enol–keto transformation goes through different mechanisms leading to multiple reaction rates.

Steady-state calculations indicate that the transition state is about 3.6 eV above the ground-enol-S_0 state. According to the absorption spectrum, shown in Fig. 3, only a small fraction of the population determined by the initial wave packet has energy above the transition state. Therefore, the overall initial reaction rate is determined by tunneling through a shallow barrier leading to the quick buildup of the keto population to about 20% in the first 50 fs, while the rest of the molecules evolve the keto population from 20% to 60% in the next 400–500 fs. Pump-probe experiments show that the reaction time scales range from 30 to 170 fs, depending on the different experimental conditions.[17–23] According to our calculations, these experimental values are all consistent since it would be difficult to control precisely how many molecules were excited above (or below) the transition state as determined by the different experi-

mental setups. Discrepancies in the reaction time scales could also be caused by technical details in interpreting the data. Remarkably, all the experiments have shown that the probing signals reach equilibrium in about 400–600 fs, which is well reproduced by both the MP/SOFT and TDSCF calculations.

Although the MP/SOFT and TDSCF calculations agree qualitatively on the trend of the enol-to-keto transfer, substantial differences exist between the two sets of calculations regarding the quantum dynamical features. Figure 4 shows that in the first 50 fs, which we have characterized as predominately tunneling through a shallow barrier, the transfer rate obtained from the TDSCF calculations is much faster than that obtained from the MP/SOFT calculations, but the TDSCF reaction rate is abruptly slowed down at 30 fs. This might be due to the limitations of the TDSCF method for properly describing interference effects associated with recrossing events. A similar situation has been observed in our previous work on the ESIPT of HPO,[15] where we have shown that the reaction rate obtained with the TDSCF method is faster than with full quantum mechanical calculations. On the other hand, the keto population obtained from MP/SOFT calculations shows a smooth change of the reaction rate, clearly resembling the experimental time-resolved spectrum measuring the keto formation, as shown in fig. 2 of ref 18.

Another difference between the MP/SOFT and the TDSCF results can be observed in the oscillations of the keto population. Experimental studies have attributed these oscillations to the low-frequency modes that modulate the proton transfer, particularly the lowest frequency internal bending mode (120 cm^{-1}). Such pronounced oscillations have also been observed in other proton transfer systems. Compared to the experimental results, the oscillations in the TDSCF simulations are too small to reflect any effect of the low-frequency modes modulating the proton transfer dynamics. In contrast, the MP/SOFT results display oscillations with intensities and time scales that partially agree with the motion of the 120, 254, 289, and 529 cm^{-1} modes.[18–19] The detailed vibrational analysis, however, is beyond the scope of the current publication and will be presented elsewhere.

To further analyze the interaction between the hydrogen motion as coupled to the other vibrational modes, we have calculated the trace of the square of the reduced density matrix $Tr[\rho^2(t)]$ associated with the r_1 coordinate, after integrating out the other degrees of freedom. For separable dynamics, $Tr[\rho^2(t)] = 1$ since the state of the r_1 coordinate remains pure. However, as the motion of r_1 couples to the other coordinates (e.g., during vibrational energy redistribution) the state of r_1 becomes mixed and $Tr[\rho^2(t)]$ decreases. Thus, the quantity $Tr[\rho^2(t)]$ serves as a standard measure of decoherence and mixing of r_1 with the other modes in the system.[13,107,108] Figure 4 shows the $Tr[\rho^2(t)]$, dropping to about 50% in just 30 fs, coincident with the quick increase of the keto population, and then, slowly decaying to 30% with small oscillations. Figure 4 clearly demonstrates that the proton transfer dynamics is strongly influenced by the coupling between the OH-stretching motion and the other vibrational modes. At the very beginning, the OH-stretching mode dissipates energy to the other modes, slowing down the reaction, but at later times proton transfer is induced by energy transfer from the other coordinates.

Figure 5 shows the evolution of the nuclear wave

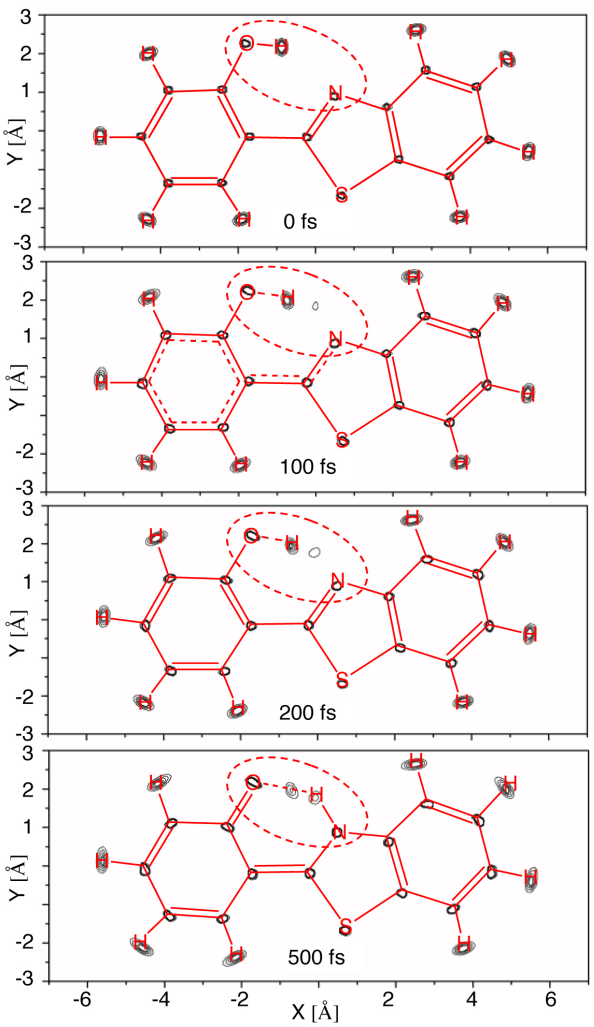

Fig. 5. MP/SOFT total probability densities $\rho_t(X,Y) = \Psi_t(X,Y)^*\Psi_t(X,Y)$ at $t = 0$, 100, 200, and 500 fs after photoexcitation of the HBT, represented as equally spaced contour levels at 2, 4, 6, and 8. The evolution of probability density shows that the keto tautomer is formed in less than 100 fs and the keto population continues building up as a result of vibrational energy redistribution in hundreds of femtoseconds.

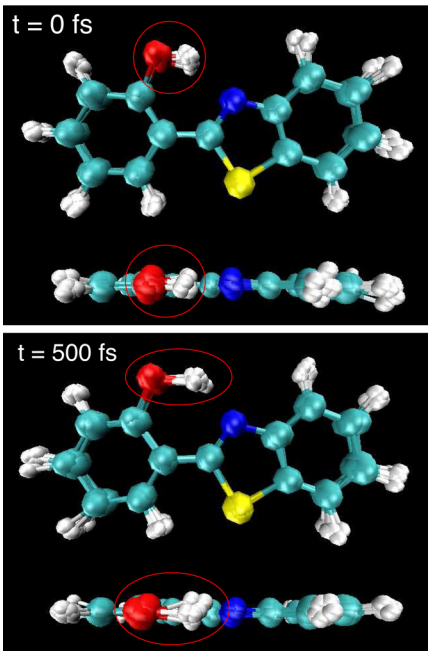

Fig. 6. Superposition of representative configurations of HBT at $t = 0$ (*top panel*) and at 500 fs after photoexcitation of the system. Each panel represents the molecule in the standard orientation (i.e., in the (x,y) plane of the page) and in the (x,z) plane to show that the molecule does not exhibit out-of-plane deformations.

packet during the first 500 fs of dynamics as represented by the total probability density in the *xy* plane of the molecule in the standard orientation:

$$\rho(X,Y) = \sum_{j=1}^{N} \int dx_1 \int dy_1 \int dz_1 \cdots \int dx_N \int dy_N \int dz_N \delta(X - x_j)\delta(Y - y_j) \times \rho(x_1, y_1, z_1, x_2, y_2, z_2 \cdots, x_N, y_N, z_N) \quad (18)$$

Such a representation is particularly insightful since the equilibrium configuration of the initial state is in the *xy* plane and the molecule remains mostly planar during the ESIPT reaction, except for small-amplitude OH wagging out-of-the plane fluctuations (see Fig. 6). Note that the contour plots of the probability density have peaks in Fig. 5 that can be easily assigned to the identities of the atoms, according to Fig. 1. In particular, the motion of the H atom transferring from the hydroxyphenyl to the benzothiazole moiety is clearly shown in terms of a bimodal distribution of enol and keto configurations with small-amplitude motions for the remaining atoms in the HBT molecule.

Figure 7 shows the evolution of the distribution of electron density for the average geometry of HBT in the S_1 state, during the first 800 fs of ESIPT dynamics after photoexcitation of the enol tautomer. Blue and

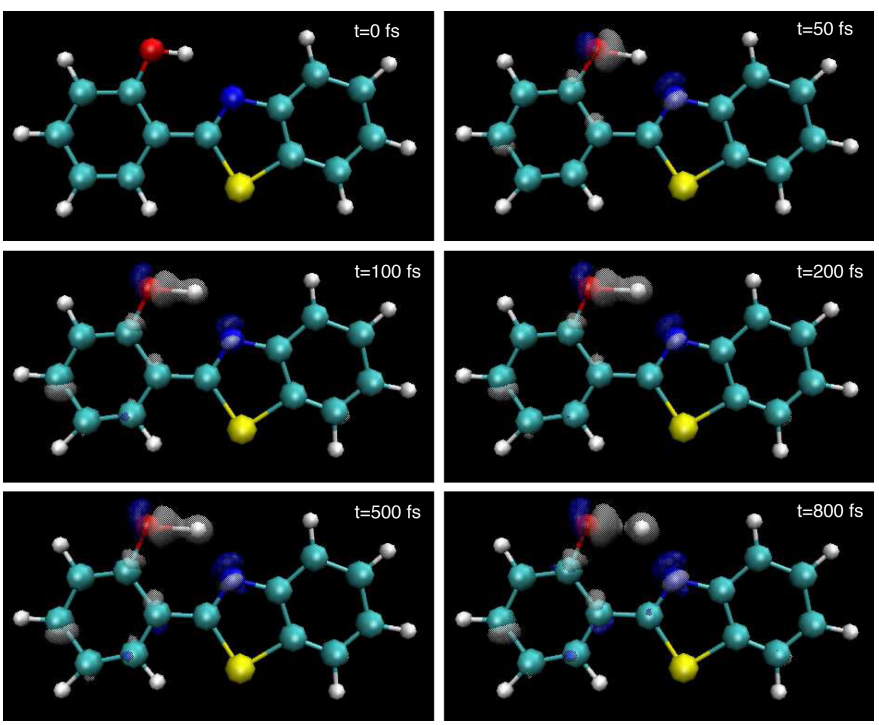

Fig. 7. Evolution of the electron density differences, relative to the charge distribution at $t = 0$, for the time-dependent mean configuration of HBT in the S_1 state. Blue and gray isosurfaces represent an increase and decrease of electronic density, respectively. It is shown that the average position of the proton evolves over hundreds of femtoseconds, after the initial electron transfer from the hydroxyphenyl moiety to the benzothiazole group through the conjugated system.

gray isosurfaces represent, respectively, an increase and decrease of electronic density relative to the distribution of electronic charge at $t = 0$ after photoexcitation. Note the decrease of electronic density in the OH bond, even at the very early time after photoexcitation of the system, and the redistribution of charge that decreases the OH bond order, forming the proton, and building up electronic density in the sp^2 orbital of the N atom. These changes suggest that the net hydrogen transfer results from an initial photoinduced electron transfer through the conjugated system linking the hydroxyphenyl and benzothiazole moieties, followed by ESIPT. Note that the average position of the proton quickly stretches out in about 50 fs and continues evolving for several hundreds of femtoseconds as vibrational energy redistribution equilibrates the ratio of enol and keto populations.

CONCLUSIONS

In this paper we have investigated the ultrafast ESIPT reaction associated with the enol–keto tautomerization reaction of HBT, using a full quantum dynamics method implemented in conjunction with a full-dimensional ab initio potential energy surface. The MP/SOFT method recursively applies the time-evolution operator as defined by the Trotter expansion to the second order accuracy in dynamically adaptive coherent-state representations. Such representations are particularly suitable for high-dimensional calculations since they allow for the analytical implementation of the Trotter expansion, bypassing the exponential scaling problem associated with usual Fourier transform in grid-based methods. Therefore, the reported calculations provide insight on the nature of quantum dynamics without invoking any kind of classical or semiclassical approximation, or a reduced dimensional model.

The MP/SOFT calculations were focused on the propagation of the 69-dimensional wave packet evolving on the ab initio excited electronic S_1 state PES to obtain a description of ESIPT at the detailed molecular level, including a detailed description of the evolution of nuclear coordinates, quantum mechanical survival amplitudes, the photoabsorption spectrum, the time-dependent keto product population, and the decoherence measure $\mathrm{Tr}[\rho^2(t)]$ characterizing the nature of hydrogen transfer as coupled to the remaining degrees of freedom in the system. The reported results are in very good agreement with experiments in almost all aspects, demonstrating both the accuracy of the MP/SOFT method and the validity of the full-dimensional model Hamiltonian for describing the ESIPT reaction in HBT. These simulations complement ultrafast spectroscopic measurements by providing fundamental insight on the nature of reaction dynamics directly, ruling out the variance caused by specific experimental conditions, and providing information at the detailed molecular level in addition to direct comparisons with experimental observables.

The MP/SOFT calculations show that maximum absorption occurs at 344 nm, in good agreement with experimental data, suggesting that the MP/SOFT methodology properly describes the effect of ESIPT on the photoabsorption of HBT when applied in conjunction with the ab initio system-bath model Hamiltonian. In agreement with time-resolved spectroscopic measurements, the simulations also predict multiple time scales for the ultrafast formation of the keto tautomer, with transfer of 15–30% population in just 30–50 fs and further increase of the keto population to about 60% in the next 400–500 fs, as modulated by multiple vibrational modes that change the distance O···N between the proton donor hydroxyphenyl and the acceptor benzothiazole moieties. The separation of time scales suggests that a small effective energy barrier separates the enol and keto tautomers in the S_1 PES along the OH reaction coordinate. Molecules with enough energy to go over the barrier would transfer to the keto form in about 4 fs (i.e., the half-period of the OH vibration). However, most of the initial transfer is due to tunneling through a shallow energy barrier during the first 50 fs, while molecules with lower energy along the reaction coordinate transfer the proton only after being activated by vibrational energy redistribution. Thus the enol–keto transformation involves different mechanisms leading to multiple reaction time scales. The strong quantum mechanical effects shown in the calculated keto populations indicate that the reaction cannot be simply described by a first-order decay. It also suggests that previously reported reaction time scales in the range of 30–170 fs are all consistent within the variations of the experimental setups. However, contrary to the interpretation of ultrafast spectroscopic measurements,[22,23] the MP/SOFT calculations do not show evidence for ESIPT as coupled to out-of-plane deformation of HBT, except for small-amplitude OH wagging out-of-the plane fluctuations. Work in progress involves the complete analysis of the vibrational spectroscopy of HBT in the S_1, as directly correlated to experimental data.

Acknowledgments. V.S.B. acknowledges a generous allocation of DOE supercomputer time from the National Energy Research Scientific Computing Center (NERSC) and financial support from grants NSF CHE 0345984, NSF ECCS 0404191, DOE DE-FG02-07ER15909, NIH 2R01-GM043278, and the United States-Israel Binational Science Foundation (BSF) R-08164. The work at Georgia Tech has been supported by the National Science Foundation (in the framework of the CRIF

Program under award CHE-0443564) and Solvay. The authors thank Robert C. Snoeberger for having computed the HBT electronic density differences reported in Fig. 7.

REFERENCES AND NOTES

(1) Zhong, D.P.; Douhal, A.; Zewail, A.H. *Proc. Natl. Acad. Sci. U.S.A.* **2000**, *97*, 14056–14061.
(2) Chattoraj, M.; King, B.A.; Bublitz, G.U.; Boxer, S.G. *Proc. Natl. Acad. Sci. U.S.A.* **1996**, *93*, 8362–8367.
(3) Miskovsky, P. *Int. J. Photoenergy* **2002**, *4*, 45–50.
(4) Haddon, R.C.; Stillinger, F.H. In *Molecular Electronic Devices*; Carter, F.L., Ed.; Marcel Dekker: New York, 1987.
(5) Parthenopoulos, D.A.; McMorrow, D.; Kasha, M. *J. Phys. Chem.* **1991**, *95*, 2668–2674.
(6) Moller, S.; Andersen, K.B.; Spanget-Larsen, J.; Waluk, J. *Chem. Phys. Lett.* **1998**, *291*, 51–56.
(7) Wu, Y.; Batista, V.S. *J. Chem. Phys.* **2004**, *121*, 1676–1680.
(8) Wu, Y.; Herman, M.F.; Batista, V.S. *J. Chem. Phys.* **2005**, *122*, Art. No, 114114.
(9) Chen, X.; Wu, Y.; Batista, V.S. *J. Chem. Phys.* **2005**, *122*, Art. No. 64102.
(10) Wu, Y.; Batista, V.S. *J. Chem. Phys.* **2003**, *118*, 6720–6724.
(11) Wu, Y.; Batista, V.S. *J. Chem. Phys.* **2003**, *119*, 7606–7606.
(12) Carrington, T. C.; Miller, W.H. *J. Chem. Phys.* **1986**, *84*, 4364–4370.
(13) Batista, V.S.; Brumer, P. *Phys. Rev. Lett.* **2002**, *89*, 143201.
(14) Guallar, V.; Batista, V.S.; Miller, W.H. *J. Chem. Phys.* **1999**, *110*, 9922–9936.
(15) Wu, Y.; Batista, V.S. *J. Chem. Phys.* **2006**, *124*, 224305.
(16) Guallar, V.; Batista, V.S.; Miller, W.H. *J. Chem. Phys.* **2000**, *113*, 9510–9522.
(17) Elsaesser, T.; Kaiser, W. *Chem. Phys. Lett.* **1986**, *128*, 231–237.
(18) Lasermer, F.; Elsaesser, T.; Kaiser, W. *Chem. Phys. Lett.* **1988**, *148*, 119–124.
(19) Lochbrunner, S.; Wurzer, A.J.; Riedle, E. *J. Phys. Chem. A* **2003**, *107*, 10580–10590.
(20) Nibbering, E.T.; Fidder, H.; Pines, E. *Annu. Rev. Phys. Chem.* **2005**, *56*, 337–367.
(21) Pfeier, M.; Lenz, K.; Lau, A.; Elsaesser, T. *J. Raman Spec.* **1997**, *28*, 61–72.
(22) Rini, M.; Dreyer, J.; Nibbering, E.T.; Elsaesser, T. *Chem. Phys. Lett.* **2003**, *374*, 13–19.
(23) Rini, M.; Kummrow, A.; Jens Dreyer, E.T.J.N.; Elsaesser, T. *Faraday Discuss.* **2002**, *122*, 27–40.
(24) Seo, J.; Kim, S.; Park, S.Y. *J. Am. Chem. Soc.* **2004**, *126*, 11154–11155.
(25) Herek, J.L.; Pedersen, S.; Banares, L.; Zewail, A.H. *J. Chem. Phys.* **1992**, *97*, 9046–9061.
(26) Frey, W.; Laermer, F.; Elsaesser, T. *J. Phys. Chem.* **1991**, *95*, 10391–10395.
(27) Lochbrunner, S.; Stock, K.; Riedle, E. *J. Mol. Struct.* **2004**, *700*, 13–18.
(28) Chudoba, C.; Riedle, E.; Pfeiffer, M.; Elsaesser, T. *Chem. Phys. Lett.* **1996**, *263*, 622–628.
(29) Fiebig, T.; Chachisvilis, M.; Manger, M.; Zewail, A.H.; Douhal, A.; Garcia-Ochoa, I.; Ayuso, A.D.H. *J. Phys. Chem. A* **1999**, *103*, 7419–7431.
(30) Ameer-Beg, S.; Ormson, S.M.; Brown, R.G.; Matousek, P.; Towrie, M.; Nibbering, E.T.J.; Foggi, P.; Neuwahl, F.V.R. *J. Phys. Chem. A* **2001**, *105*, 3709–3718.
(31) Bader, A.N.; Pivovarenko, V.G.; Demchenko, A.P.; Ariese, F.; Gooijer, C. *J. Phys. Chem. B* **2004**, *108*, 10589–10595.
(32) Toele, P.; Glasbeek, M. *Chem. Phys. Lett.* **2005**, *407*, 487–492.
(33) Sakota, K.; Okabe, C.; Nishi, N.; Sekiya, H. *J. Phys. Chem. A* **2005**, *109*, 5245–5247.
(34) Nagashima, U.; Nagaoka, S.; Katsumata, S. *J. Phys. Chem.* **1991**, *95*, 3532–3538.
(35) Sobolewski, A.L.; Domcke, W. *Chem. Phys. Lett.* **1993**, *211*, 82–87.
(36) Duan, X.F.; Scheiner, S. *Chem. Phys. Lett.* **1993**, *204*, 36–44.
(37) Guallar, V.; Moreno, M.; Lluch, J.M.; Amat-Guerri, F.; Douhal, A. *J. Phys. Chem.* **1996**, *100*, 19789–19794.
(38) Sobolewski, A.L.; Domcke, W. *Chem. Phys. Lett.* **1999**, *300*, 533–539.
(39) Scheiner, S. *J. Phys. Chem. A* **2000**, *104*, 5898–5909.
(40) Granucci, G.; Hynes, J.T.; Millie, P.; Tran-Thi, T.H. *J. Am. Chem. Soc.* **2000**, *122*, 12243–12253.
(41) Casadesus, R.; Moreno, M.; Lluch, J.M. *Chem. Phys. Lett.* **2002**, *356*, 423–430.
(42) Roscioli, J.R.; Pratt, D.W.; Smedarchina, Z.; Siebrand, W.; Fernandez-Ramos, A. *J. Chem. Phys.* **2004**, *120*, 11351–11354.
(43) Vendrell, O.; Moreno, M.; Lluch, J.M.; Hammes-Schiffer, S. *J. Phys. Chem. B* **2004**, *108*, 6616–6623.
(44) Abou-Zied, O.K.; Jimenez, R.; Thompson, E.H.Z.; Millar, D.P.; Romesberg, F.E. *J. Phys. Chem. A* **2002**, *106*, 3665.
(45) Dohual, A.; Lahmani, F.; Zehnacker-Rontien, A.; Amat-Guerri, F. In *Fast Elementary Processes in Chemical and Biological Systems. AIP Conf. Proc. 346*; Tramer, X., Ed.; American Institute of Physics: New York, 1995.
(46) Makri, N. *Annu. Rev. Phys. Chem.* **1999**, *50*, 167–191, and references therein.
(47) Beck, M.H.; Jackle, A.; Worth, G.A.; Meyer, H.D. *Phys. Rep. -Rev. Sec. Phys. Lett.* **2000**, *324*, 1–105.
(48) Miller, W.H. *Proc. Natl. Acad. Sci. U.S.A.* **2005**, *102*, 6660–6664.
(49) Ben-Nun, M.; Quenneville, J.; Martinez, T.J. *J. Phys. Chem. A* **2000**, *104*, 5161–5175.
(50) Ben-Nun, M.; Martinez, T.J. *Adv. Chem. Phys.* **2002**, *121*, 439–512.
(51) Kim, S.Y.; Hammes-Schiffer, S. *J. Chem. Phys.* **2003**, *119*, 4389–4398.
(52) Wang, H.B.; Thoss, M. *J. Phys. Chem. A* **2003**, *107*, 2126–2136.

(53) Nguyen, P.H.; Stock, G. *J. Chem. Phys.* **2003**, *119*, 11350–11358.
(54) Shalashilin, D.V.; Child, M.S. *Chem. Phys.* **2004**, *304*, 103–120.
(55) Shi, Q.; Geva, E. *J. Chem. Phys.* **2004**, *121*, 3393–3404.
(56) Donoso, A.; Martens, C.C. *J. Chem. Phys.* **2002**, *116*, 10598–10605.
(57) Prezhdo, O.V.; Pereverzev, Y.V. *J. Chem. Phys.* **2000**, *113*, 6557–6565.
(58) Hone, T.D.; Voth, G.A. *J. Chem. Phys.* **2004**, *121*, 6412–6422.
(59) Bonella, S.; Coker, D.F. *J. Chem. Phys.* **2001**, *114*, 7778–7789.
(60) Cardenas, A.E.; Krems, R.; Coalson, R.D. *J. Phys. Chem. A* **1999**, *103*, 9469–9474.
(61) Turi, L.; Rossky, P.J. *J. Chem. Phys.* **2004**, *120*, 3688–3698.
(62) Nest, M.; Saalfrank, P. *Chem. Phys.* **2001**, *268*, 65–78.
(63) Jang, S.J.; Cao, J.S. *J. Chem. Phys.* **2001**, *114*, 9959–9968.
(64) Sergi, A.; MacKernan, D.; Ciccotti, G.; Kapral, R. *Theor. Chem. Acc.* **2003**, *110*, 49–58.
(65) Makarov, D.E.; Metiu, H. *J. Chem. Phys.* **1999**, *111*, 10126–10136.
(66) Zhang, S.S.; Pollak, E. *J. Chem. Phys.* **2003**, *119*, 11058–11063.
(67) Antoniou, D.; Schwartz, S.D. *J. Chem. Phys.* **2003**, *119*, 11329–11334.
(68) Gao, J.L.; Truhlar, D.G. *Annu. Rev. Phys. Chem.* **2002**, *53*, 467–505.
(69) Olsson, M.H.M.; Siegbahn, P.E.M.; Warshel, A. *J. Am. Chem. Soc.* **2004**, *126*, 2820–2828.
(70) Craig, I.R.; Manolopoulos, D.E. *J. Chem. Phys.* **2004**, *121*, 3368–3373.
(71) Neuhauser, D. *J. Chem. Phys.* **1994**, *100*, 9272–9275.
(72) Zhu, W.; Zhang, J.Z.H.; Zhang, D.H. *Chem. Phys. Lett.* **1998**, *292*, 46–50.
(73) Schatz, G.C.; Fitzcharles, M.S.; Harding, L.B. *Faraday Discuss.* **1987**, *84*, 359–369.
(74) Clary, D.C. *J. Phys. Chem.* **1994**, *98*, 10678–10688.
(75) Kosloff, R. *Annu. Rev. Phys. Chem.* **1994**, *45*, 145–178.
(76) Fair, J.R.; Schaefer, D.; Kosloff, R.; Nesbitt, D.J. *J. Chem. Phys.* **2002**, *116*, 1406–1416.
(77) Echave, J.; Clary, D.C. *J. Chem. Phys.* **1994**, *100*, 402–422.
(78) Yu, H.G.; Muckerman, J.T. *J. Chem. Phys.* **2002**, *117*, 11139–11145.
(79) Hernandez, M.I.; Clary, D.C. *J. Chem. Phys.* **1994**, *101*, 2779–2784.
(80) Charlo, D.; Clary, D.C. *J. Chem. Phys.* **2002**, *117*, 1660–1672.
(81) Bowman, J.M. *J. Phys. Chem. A* **1998**, *102*, 3006–3017.
(82) Xie, D.Q.; Chen, R.Q.; Guo, H.A. *J. Chem. Phys.* **2000**, *112*, 5263–5269.
(83) Anderson, S.M.; Park, T.J.; Neuhauser, D. *Phys. Chem. Chem. Phys.* **1999**, *1*, 1343–1349.
(84) Feit, M.D.; Fleck, J.A.; Steiger, A. *J. Comput. Phys.* **1982**, *47*, 412–433.
(85) Feit, M.D.; Fleck, J.A. *J. Chem. Phys.* **1983**, *78*, 301–308.
(86) Kosloff, D.; Kosloff, R. *J. Comput. Phys.* **1983**, *52*, 35–53.
(87) Tal-Ezer, H.; Kosloff, R. *J. Chem. Phys.* **1984**, *81*, 3967–3971.
(88) Park, T.J.; Light, J.C. *J. Chem. Rev.* **1986**, *85*, 5870–5876.
(89) Herman, M.F.; Kluk, E. *Chem. Phys.* **1984**, *91*, 27–34.
(90) Makri, N.; Thompson, K. *J. Chem. Phys.* **1999**, *110*, 1343–1353.
(91) Mallat, S.G.; Zhang, Z. F. *IEEE Trans. Signal Process.* **1993**, *41*, 3397–3415.
(92) Heller, E.J. *Chem. Phys. Lett.* **1975**, *34*, 321–325.
(93) Davis, M.J.; Heller, E.J. *J. Chem. Phys.* **1979**, *71*, 3383–3395.
(94) Heller, E.J. *J. Chem. Phys.* **1981**, *75*, 2923–2931.
(95) Coalson, R.D.; Karplus, M. *Chem. Phys. Lett.* **1982**, *90*, 301–305.
(96) Sawada, S.I.; Heather, R.; Jackson, B.; Metiu, H. *Chem. Phys. Lett.* **1985**, *83*, 3009–3027.
(97) Kay, K.G. *J. Chem. Phys.* **1989**, *91*, 170–179.
(98) Shalashilin, D.V.; Jackson, B. *Chem. Phys. Lett.* **1998**, *291*, 143–152.
(99) Andersson, L.M. *J. Chem. Phys.* **2001**, *115*, 1158–1165.
(100) Shalashilin, D.V.; Child, M.S. *J. Chem. Phys.* **2000**, *113*, 10028–10036.
(101) Shalashilin, D.V.; Child, M.S. *J. Chem. Phys.* **2001**, *115*, 5367–5375.
(102) Gerber, R.B.; Buch, V.; Ratner, M.A. *J. Chem. Phys.* **1982**, *77*, 3022–3030.
(103) Frisch, M.J.; et al. *Gaussian 03, Revision C.02*. Gaussian, Inc., Wallingford, CT, 2004.
(104) Flores, S.; Batista, V.S. *J. Phys. Chem. B* **2003**, *108*, 6745–6749.
(105) Swope, W.; Andersen, H.; Berens, P.; Wilson, K. *J. Chem. Phys.* **1982**, *76*, 637–649.
(106) Heller, E.J. *J. Chem. Phys.* **1976**, *65*, 1289–1298.
(107) Joos, E.; Zeh, H.D. *Phys. Rev. B: Condens. Matter* **1985**, *59*, 223.
(108) Zurek, W.H. *Phys. Rev. D* **1981**, *26*, 1862.